ORIGINAL ARTICLE

Three-Dimensional Heart Segmentation and Absolute Quantitation of Cardiac ^{123}I-metaiodobenzylguanidine Sympathetic Imaging Using SPECT/CT

Shintaro Saito, MD, PhD[1], Kenichi Nakajima, MD, PhD[2], Takayuki Shibutani, RT, PhD[3], Hiroshi Wakabayashi, MD, PhD[1], Hiroto Yoneyama, RT, PhD[4], Takahiro Konishi, RT[4], Hiroshi Mori, MD, PhD[1], Aki Takata, MD[1], and Seigo Kinuya, MD, PhD[1]

Received: May 31, 2023/Revised manuscript received: July 31, 2023/Accepted: September 3, 2023

Abstract

***Background*: A three-dimensional (3D) approach to absolute quantitation of ^{123}I-metaiodobenzylguanidine (MIBG) sympathetic nerve imaging using single-photon emission tomography (SPECT) / computed tomography (CT) is not available. Therefore, we calculated absolute cardiac counts and standardized uptake values (SUVs) from images of 72 consecutive patients with cardiac and neurological diseases using ^{123}I-MIBG SPECT/CT and compared them with conventional planar quantitation. We aimed to develop new methods for 3D heart segmentation and the quantitation of these diseases.**

***Methods*: We manually segmented early and late SPECT/CT images of the heart in 3D, then calculated mean (SUV_{mean}) and maximum (SUV_{max}) SUVs. We analyzed correlations between SUVs and planar heart-to-mediastinum ratios (HMRs), and between washout rates (WRs) derived from the SUVs and planar data. We also categorized WRs as normal or abnormal using linear regression lines determined by the relationship between SPECT/CT and planar WRs, and assessed agreement between them.**

***Results*: We calculated SUV_{mean} and SUV_{max} from all early and late ^{123}I-MIBG SPECT/CT images. Planar HMRs correlated with early and late SUV_{mean} ($R^2 = 0.59$ and 0.73, respectively) and SUV_{max} ($R^2 = 0.46$ and 0.60, respectively; both $p<0.0001$). The SPECT/CT WRs determined based on SUV_{mean} and SUV_{max} ($R^2=0.79$ and 0.45, $p<0.0001$) closely correlated with planar WRs. Agreement of high and low WRs between planar WRs and SPECT/CT WRs calculated using SUV_{max} and SUV_{mean} reached 88.1% and 94.4% respectively.**

***Conclusions*: We found that sympathetic nervous activity could be absolutely quantified in 3D from ^{123}I-MIBG SPECT/CT images. Therefore, we propose a new method for quantifying sympathetic innervation on SPECT/CT images.**

Keywords: Cardiac innervation imaging, Heart-to-mediastinum ratio, Neurodegenerative disease, Quantitation method, Standardized uptake value, Washout rate

Ann Nucl Cardiol 2023; 9 (1): 61–67

Cardiac ^{123}I-metaiodobenzylguanidine (MIBG) scintigraphy is an established practical method for assessing global and regional cardiac sympathetic innervation (1–4). Myocardial ^{123}I-MIBG uptake and washout are clinically valuable indicators, particularly for assessing severity and prognosis, therapeutic effects on heart failure, and arrhythmogenic disease (5–9). Neurodegenerative diseases such as dementia with Lewy bodies (DLB) and Parkinson's disease (PD) are also common indications for assessment by ^{123}I-MIBG scintigraphy (10–13).

DOI: 10.17996/anc.23-00002

1) Department of Nuclear Medicine, Kanazawa University, Kanazawa, Japan
2) Department of Functional Imaging and Artificial Intelligence, Kanazawa University, Kanazawa, Japan
3) Department of Quantum Medical Technology, Institute of Medical, Pharmaceutical and Health Sciences, Kanazawa University, Kanazawa, Japan
4) Department of Radiological Technology, Kanazawa University Hospital, Kanazawa, Japan

Table 1 Clinical characteristics of 72 patients

Characteristics	Values
Male (%)	31 (43%)
Age (y)	66.7 ± 12.3
Body weight (kg)	59.5 ± 18.4
Body mass index (kg/m^2)	23.9 ± 6.0
Patients with cardiac diseases	15 (21%)
Cardiomyopathy	3
Chronic heart failure	2
Suspected ischemic heart disease	10
Patients with neurological diseases (n, %)	57 (79%)
Parkinson's syndrome	22
Parkinson's disease	5
Dementia with Lewy bodies	2
Familial amyloid polyneuropathy	6
Non-PS/PD/DLB	22
Reduced cardiac uptake	10 (14%)
Left ventricular ejection fraction (%)	62.5 ± 11.6

Unless otherwise specified, data are presented as n, n (%), or means ± standard deviation.

However, the conventional approach to defining regions of interest (ROIs) can result in up to 40% of the data being located in a gray area close to the boundary through which normal and pathological innervation are differentiated in the clinical setting (14). Heart-to-mediastinum ratios (HMRs) and washout rates (WRs) have been computed from planar images in Japan using the semiautomated software smartMIBG created in a collaboration (FUJIFILM Toyama Chemical Co. Ltd., Tokyo, Japan and PDRadiopharma Inc., Tokyo, Japan) that sets ROIs for HMR and WR calculations (15). The ROIs could also be manually set according to the American Society of Nuclear Cardiology and European guidelines (16–18).

Three-dimensional (3D) images acquired using single-photon emission tomography (SPECT) provide a more comprehensive representation of localized cardiac sympathetic innervation than HMRs derived from two-dimensional (2D) planar images (1, 19). Degrees of segmental defects can also be quantified using the 17-segment model applied in myocardial perfusion imaging (5). However, the capability of quantitative evaluation remains limited, and SPECT is not routine in clinical practice. The significance of quantitative SPECT/computed tomography (CT) is increasing. Because SPECT/CT is effective for dosimetry after radionuclide therapy, a theranostics concept has become established (20). Moreover, SPECT/CT has recently been applied to bone, cardiac, and brain imaging. However, a 3D method of absolute quantitation has not been established for SPECT/CT sympathetic nerve imaging using ^{123}I-MIBG.

Therefore, we compared values generated by conventional planar image-based quantitation with absolute heart counts determined as mean and maximum standardized uptake values (SUVs) derived from ^{123}I-MIBG SPECT images with low-dose CT for attenuation correction.

Methods

Patients

We enrolled 72 consecutive patients (male, 31; female, 41; average age 66.7 ± 12.3 y; range, 35–88 y) with cardiac (n=15) and neurological (n=57) diseases at Kanazawa University Hospital during 2020 and 2021. Table 1 shows that these diseases comprised cardiomyopathy (n = 3), chronic heart failure (n=2), and suspected ischemic heart disease (n=10). The neurological diseases comprised Parkinson's syndrome (PS; n = 22), PD (n = 5), DLB (n = 2), familial amyloid polyneuropathy (n = 6), and non-PS/PD/DLB (n = 22). The results of ^{123}I-MIBG planar and SPECT/CT imaging revealed a significant decrease in cardiac ^{123}I-MIBG uptake in 10 patients (HMRs<1.5). Left ventricular ejection fraction assessment by echocardiography (n=47) was 62.5% ± 11.6% (14%–78%). This information was not available for 25 patients with neurological disorders.

^{123}I-MIBG imaging

All patients were assessed by early and late ^{123}I-MIBG planar and SPECT/CT imaging using a Symbia Intevo and a Symbia Intevo Bold SPECT/CT scanner (Siemens Healthcare, Erlangen, Germany) with a medium-energy collimator. The patients were intravenously injected with 111 MBq of ^{123}I-MIBG, then images were acquired at 15–20 min (early phase) and at 180–240 min (late phase). Planar images were acquired for 5 min under the following conditions: matrix, 256 × 256; pixel size 2.4 mm; zoom factor, 1.0. The SPECT images were acquired for 30 s per view under the following conditions: matrix, 128 × 128, pixel size, 4.8 mm; zoom factor, 1.0; projections, 60; circular orbit, 360° ; and rotation radius, 24 cm. The SPECT data were reconstructed using an ordered subset conjugate gradient minimizer with the xSPECT Quant algorithm. After SPECT acquisition, low-dose CT images were acquired for attenuation correction under the following conditions: 130 kV; 20 mA with CARE Dose 4D; pitch, 1.5; rotation duration, 0.6 sec; collimation, 16 × 1.2. The CT-based attenuation and multi-energy-window scatter were automatically corrected.

Planar image analysis

Early and late HMRs in planar images were calculated using semiautomated smartMIBG software to set ROIs as described (15). The software algorithm uses circular heart and mediastinal ROIs that are 10% of the girth of each patient and 30% of the mediastinal height. After pointing to the center of

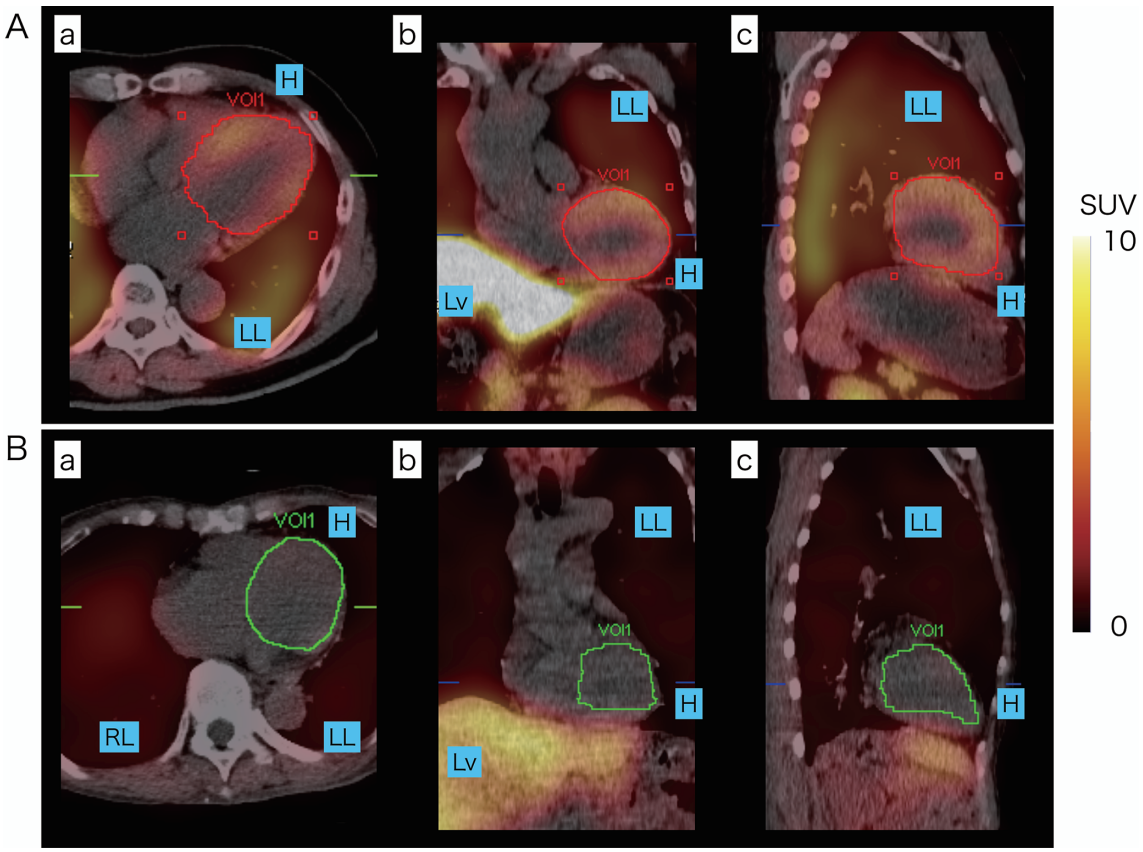

Figure 1 Manual three-dimensional left ventricular segmentation images with ^{123}I-MIBG SPECT/CT data.
Patients with moderate (A) and reduced (B) uptake. Transaxial (a), coronal (b), and sagittal (c) SPECT/CT images. Red and green lines on VOI show border of manually drawn 3D left ventricle segmentation. Maximum and mean SUVs calculated from VOIs are 5.38 and 2.59 (A), and 0.83 and 0.29 (B), respectively.
3D, three dimensional; CT, computed tomography; H, heart; LL, left lung; Lv, liver; SPECT, single photon emission computed tomography, SUV, standardized uptake value; VOI, volume of interest.

the heart, all processing is automated, with the option to add manual adjustment as needed.

We calculated WRs from early and late heart (H_E and H_L) and mediastinal (M_E and M_L) counts using the following formulae for planar WRs with mediastinal background counts and time-decay corrections:

[(Planar H_E–M_E)–(Planar H_L–M_L)/DCF]/(Planar H_E–M_E) × 100 (%),

where DCF is the decay correction factor calculated as 0.5^ (time [h] between early and late imaging/13).

Left ventricular segmentation and calculation of SUVs and WRs on SPECT/CT images

We manually segmented all 3D hearts with the ROI being the entire left ventricle on early and late SPECT/CT images. The boundary of the left ventricle was determined using SPECT, X-ray CT, and fused images, and two nuclear medicine specialists assessed both morphology and ^{123}I-MIBG activity. Figure 1 shows an example of 3D left ventricular segmentation.

We derived mean (SUV_{mean}) and maximum (SUV_{max}) from early and late SPECT/CT images based on three-dimensional left ventricular segmentation. The SUV is the normalized concentration of tissue radioactivity relative to the injected radiotracer dose and body weight. The SPECT/CT SUV_{max} represents the pixel with the highest ^{123}I-MIBG uptake activity and was calculated as:

maximum activity in the regions of interests (Bq/g)/(injected dose [Bq]/body weight [g]).

SPECT/CT SUV_{mean} was calculated as the average SUV of voxels inside a volume of interest (VOI), that comprises the entire left ventricle.

The SPECT/CT WRs were respectively calculated from SUV_{max} and SUV_{mean} as:

SPECT/CT WR SUV_{max} = (SPECT/CT Early SUV_{max} – SPECT/CT Late SUV_{max})/SPECT/CT Early SUV_{max} × 100 (%) and

SPECT/CT WR SUV_{mean} = (SPECT/CT Early SUV_{mean} – SPECT/CT Late SUV_{mean})/SPECT/CT Early SUV_{mean} × 100 (%).

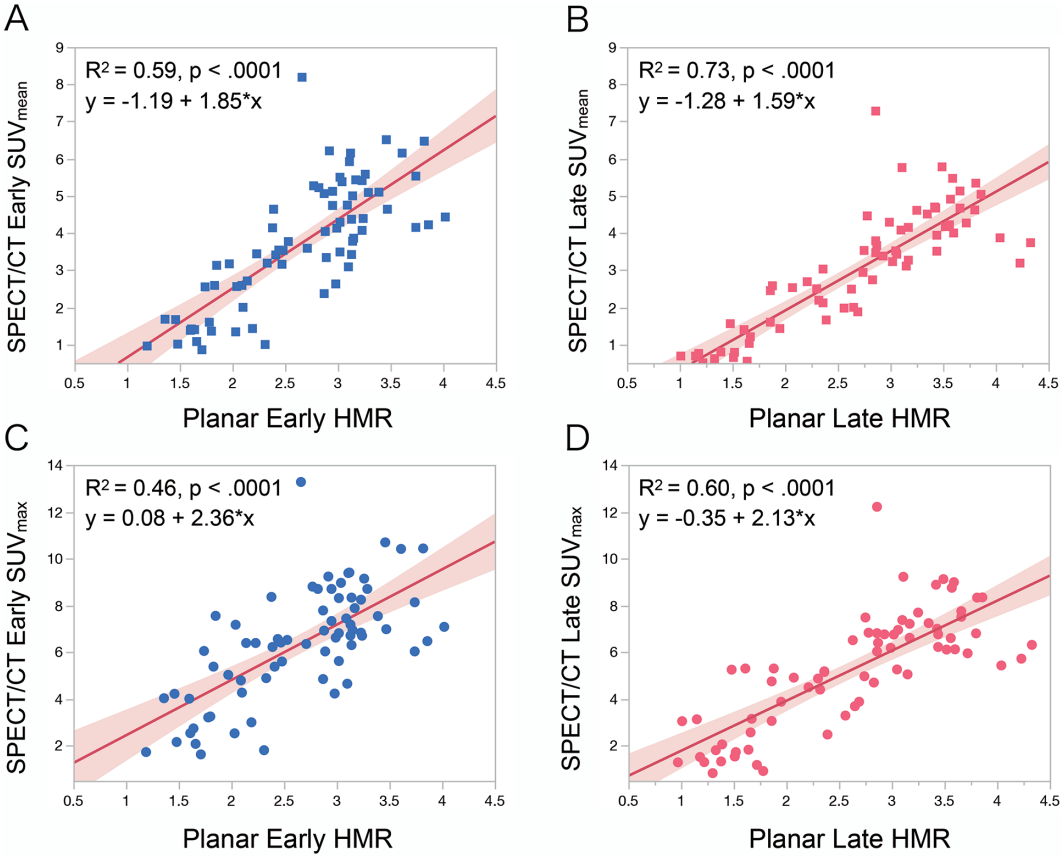

Figure 2 Relationships between SUVs calculated from ^{123}I-MIBG SPECT/CT images and HMRs from conventional planar images.

SPECT/CT early SUV_{mean} vs. planar early HMR (A); SPECT/CT late SUV_{mean} vs. planar late HMR (B); SPECT/CT early SUV_{max} vs. planar early HMR (C); SPECT/CT late SUV_{max} vs. planar late HMR (D). Shaded area, confidence of fit.

CT, computed tomography; HMR, heart-to-mediastinum; SPECT, single photon emission computed tomography; SUV, standardized uptake value.

Comparison of quantitative findings between SPECT/CT and planar images

We examined correlations between SPECT/CT SUV_{max} and SUV_{mean} and planar HMRs in the early and late images. We also analyzed correlations between WRs derived from SPECT/CT (SUV_{max} and SUV_{mean}) and planar images. The planar WR cutoff to differentiate normal from abnormal based on standard values derived from Japanese Society of Nuclear Medicine working group databases (n=62) was 34.0% (21). The SPECT/CT WR SUV_{max} and SUV_{mean} cutoff were determined based on correlations between planar and SPECT/CT WRs. We classified the patients as normal or anomalous according to the cutoff values for SPECT/CT WR and planar WR, then analyzed agreement between the methods.

Ethics approval and consent to participate

The Kanazawa University Ethics Committee approved the current investigation. The need for written informed consent from the patients was waived because this study was retrospective.

Statistical analysis

Data are shown as means and standard deviations. Differences in WRs, heart counts, SUVs, and HMRs between SPECT/CT and planar images were determined using t-tests and two-way analysis of variance. Relationships between SPECT/CT and planar techniques were analyzed using linear regression. All data were analyzed using JMP Pro version 17 (SAS Institute Inc., Cary, NC, USA). Values with $p<0.05$ were considered statistically significant.

Results

The SUV_{mean} and SUV_{max} was computed from early and late ^{123}I-MIBG SPECT/CT images from all patients. Figure 1 shows an example of SUV values determined by manual 3D left ventricle segmentation.

SPECT/CT SUV vs. planar HMR

We compared heart counts in SPECT/CT and planar images using manual 3D segmentation and the conventional method, respectively. The SPECT/CT early and late SUV_{mean} significantly correlated with planar HMRs in all patients (R^2=0.59

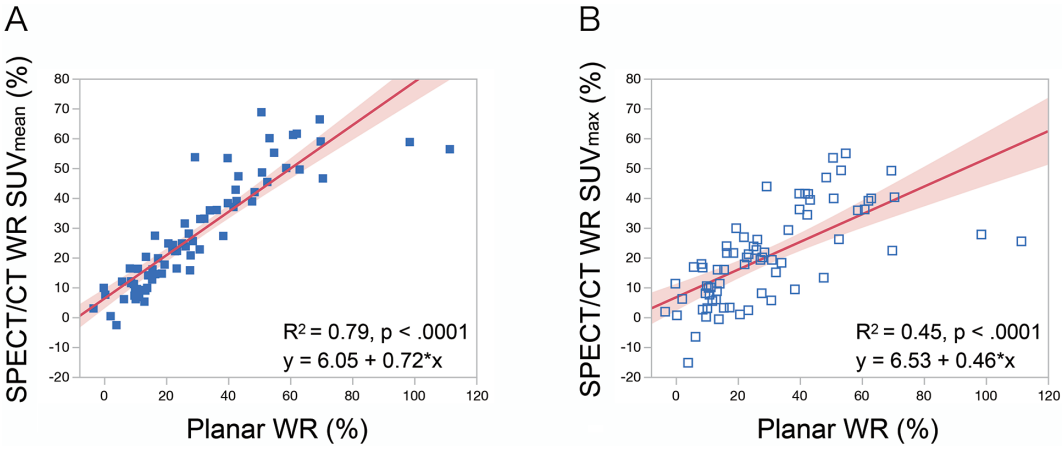

Figure 3 Relationships between WRs derived from ^{123}I-MIBG SPECT/CT images using manual heart segmentation and planar images using conventional methods.
SPECT/CT WR (A) SUV_{mean} and (B) SUV_{max} vs. planar WR. Shaded area, confidence of fit.
SPECT, single photon emission computed tomography; SUV, standardized uptake value; WR, washout rate.

Table 2 Washout rates determined from SUV derived from SPECT/CT images and standard methods using planar images

A		Planar WR		Total
		<34%	≥ 34%	
SPECT/CT WR SUV_{mean}	<30%	43 (59.7%)	1 (1.4%)	44 (61.1%)
	≥30%	3 (4.2%)	25 (34.7%)	28 (38.9%)
Total		46 (63.9%)	26 (36.1%)	72

B		Planar WR		Total
		<34%	≥ 34%	
SPECT/CT WR SUV_{max}	<30%	42 (58.3%)	4 (5.5%)	46 (63.9%)
	≥30%	4 (5.5%)	22 (30.6%)	26 (36.1%)
Total		46 (63.9%)	26 (36.1%)	72

SPECT/CT WR SUV_{mean} and SUV_{max}, SPECT/CT washout rates respectively calculated from early and late SUV_{mean} and SUV_{max}.
CT, computed tomography; SPECT, single photon emission computed tomography; SUV, standardized uptake value; WR, washout rate.

and 0.73, p<0.0001; Figure 2A). Correlations were significant between SPECT/CT SUV_{max} and planar HMRs (R^2=0.46 and 0.60, p<0.0001; Figure 2B).

SPECT/CT vs. planar WRs

We compared WRs from SPECT/CT and planar images using manual 3D segmentation and the conventional method, respectively. Correlations between SPECT/CT WRs (determined using SUV_{mean} and SUV_{max}) and planar WRs were significant (R^2=0.79 and 0.45, respectively; p<0.0001 for both; Figure 3A and B). The criteria for SPECT/CT WR using SUV_{mean} and SUV_{max} were 30% and 25%, respectively, determined as linear regression of planar WRs at the upper limit of the normal range (34%) (21). The patients were then classified as having normal or abnormal WRs based on the cutoff values of SPECT/CT WRs determined as SUV_{mean}, SUV_{max}, and planar WRs (Table 2A and B). The SPECT/CT WRs determined based on SUV_{mean} and SUV_{max} agreed with planar WRs in 68 (94.4%) and 64 (88.1%) of the 72 patients, respectively (Table 2A and B).

Discussion

These present findings showed that absolute cardiac counts and SUVs can be calculated using ^{123}I-MIBG SPECT together with low-dose CT for attenuation correction. Furthermore, SPECT/CT and planar images quantified using 3D and conventional methods significantly correlated.

Benefits of 3D over 2D conventional imaging

The diagnostic and prognostic values of HMR using ^{123}I-MIBG planar images have been validated, as planar imaging has traditionally been used to assess sympathetic nerve activity

(22). The planar approach has inherent disadvantages in terms of objectivity because the HMR is a simple metric based solely on cardiac and mediastinal regions. Data derived from 2D images cannot fully distinguish the characteristics of 3D structures such as the heart. We therefore analyzed 3D ^{123}I-MIBG SPECT images to assess average heart counts and WRs in the preceding study and found significant correlations with planar images (23). Quantified data derived from the literature have historically been relative. Here, we combined SPECT and CT to facilitate attenuation correction to facilitate SUV evaluation. In fact, recent advancements in SPECT/CT technology have led to widespread 3D image evaluation in oncology, cardiology, endocrinology, and other disciplines; thus, it should also be applicable to ^{123}I-MIBG sympathetic imaging.

Three-dimensional heart quantitation based on SUVs

Quantitation provides nuclear medicine imaging with significant advantages. The SUV has served as a basic tool for determining activity in positron emission tomography images. Although it has been applied to fluorodeoxyglucose imaging most frequently, SUVs are now also considered optimal for SPECT imaging. This has led to the development of a wide range of radiopharmaceuticals and potential applications.

In addition to disease progression or treatment response evaluation, quantitative SPECT/CT imaging surrogates can be useful to diagnose diseases and select patients before undergoing radionuclide therapy (20). The quantitation of bone tracers for orthopedic and cancer applications is evolving, and opportunities in cardiac and neurological imaging are increasing (20).

Here, we tested our hypothesis that quantifying cardiac counts and WRs from 3D ^{123}I-MIBG SPECT/CT images could be used to discriminate cardiac sympathetic neuronal function. We calculated SUV_{max} and SUV_{mean} from 3D images of the left ventricle and compared them with conventional quantitation of 2D planar images. We found that the SUV_{mean} correlated more closely than SUV_{max} with conventional 2D values. The following might provide an explanation. The HMR is calculated from planar images as the ratio of the average counts per pixel in ROIs, and the SUV_{mean} is based on the average SUV of all pixels in ROIs. The SUV_{max} is derived from a single pixel, and thus cannot not reflect an entire ROI. Considering the characteristics of SUV_{mean} and SUV_{max}, 3D quantitation using SUV_{mean} might be reasonable when assessing total accumulation in the entire heart based on ^{123}I-MIBG sympathetic images. However, since SUV_{mean} might depend on ROI definition and be subject to intra- and interobserver variations, the relationship between each of the 3D quantitative values including SUV_{mean} and SUV_{max} and clinical diagnosis and prognosis needs to be investigated in future studies.

Regarding the ROI setting for 3D quantitation, besides calculating by segmenting the entire left ventricle as in the present study, threshold-based contours using a specific ratio of the maximal value has also been used in nuclear medicine studies. However, myocardial uptake of ^{123}I-MIBG is not always homogeneous, and patients frequently have inferior defects or very low uptake. We therefore segmented the entire left ventricle rather than applying the thresholding method for more accurate 3D quantitation.

Future directions for heart segmentation

We manually segmented the left ventricles of patients to determine whether 3D quantitative values derived from SPECT/CT images were comparable with conventional 2D values. However, manual segmentation is laborious. Therefore, the introduction of artificial intelligence to automated 3D segmentation should significantly improve convenience in the near future. A convolutional neural network has been applied to the automated segmentation and quantitation of cardiac ^{123}I-MIBG SPECT images (23). We speculate that this will trigger further investigation into SPECT/CT-based automated segmentation and absolute quantitation.

Limitations

Due to our small patient cohort, more populations should be analyzed to improve the precision of heart segmentation and quantitative accuracy. Neurological and cardiac diseases have been assessed by clinical studies of ^{123}I-MIBG innervation in Japan. We aimed to develop methods for 3D heart segmentation and quantitation of both types of diseases. We assured the broad applicability of 3D heart segmentation using data from consecutive patients with a wide range of backgrounds. Some of them have yet to be definitively diagnosed with cardiac and neurological diseases. Thus, the relationship between the 3D quantitation calculated as described herein and clinical diagnosis will require further investigation.

Conclusions

Three-dimensional absolute quantitation of sympathetic nervous activity is feasible using ^{123}I-MIBG SPECT/CT images. The results significantly correlated with conventional quantitation of 2D planar images of patients with neurological and cardiac diseases. Therefore, we suggest that this method has potential for quantifying cardiac sympathetic nerve activity.

Acknowledgments

The authors thank Norma Foster (English Express, North Vancouver, BC, Canada) for editorial assistance.

Sources of funding

This study was partly funded by the G-7 Scholarship Foundation and JSPS Grant-in-Aid for Early-Career Scientists in Japan (PI: S. Saito, No. 22K15801; PI: K. Nakajima, No. 20K07990).

Conflicts of interest

KN is in a research collaboration with PDRadiopharma, Inc. Tokyo, Japan, which supplied the ^{123}I-MIBG. All other authors declare that they have no competing interests.

Reprint requests and correspondence:
Shintaro Saito, MD, PhD
Department of Nuclear Medicine, Kanazawa University, Kanazawa, Japan, 13-1 Takara-machi, Kanazawa 920-8640, Japan
E-mail: shintarosaito19861118@gmail.com

References

1. Verschure DO, Nakajima K, Verberne HJ. Cardiac ^{123}I-*m*IBG imaging in heart failure. Pharmaceuticals (Basel) 2022; 15: 656.
2. Verschure DO, Bongers V, Hagen PJ, Somsen GA, van Eck-Smit BLF, Verberne HJ. Impact of a predefined mediastinal ROI on inter-observer variability of planar ^{123}I-MIBG heart-to-mediastinum ratio. J Nucl Cardiol 2014; 21: 605–13.
3. Pellegrino T, Petretta M, De Luca S, et al. Observer reproducibility of results from a low-dose ^{123}I-metaiodobenzylguanidine cardiac imaging protocol in patients with heart failure. Eur J Nucl Med Mol Imaging 2013; 40: 1549–57.
4. Bateman TM, Ananthasubramaniam K, Berman DS, et al. Reliability of the ^{123}I-mIBG heart/mediastinum ratio: Results of a multicenter test-retest reproducibility study. J Nucl Cardiol 2019; 26: 1555–65.
5. Nakajima K, Nakata T, Doi T, et al. Validation of 2-year ^{123}I-meta-iodobenzylguanidine-based cardiac mortality risk model in chronic heart failure. Eur Heart J Cardiovasc Imaging 2018; 19: 749–56.
6. Nakata T, Nakajima K, Yamashina S, et al. A pooled analysis of multicenter cohort studies of ^{123}I-mIBG imaging of sympathetic innervation for assessment of long-term prognosis in heart failure. JACC Cardiovasc Imaging 2013; 6: 772–84.
7. Travin MI, Henzlova MJ, van Eck-Smit BLF, et al. Assessment of ^{123}I-mIBG and ^{99m}Tc-tetrofosmin single-photon emission computed tomographic images for the prediction of arrhythmic events in patients with ischemic heart failure: Intermediate severity innervation defects are associated with higher arrhythmic risk. J Nucl Cardiol 2017; 24: 377–91.
8. Nakajima K, Nakata T, Doi T, Tada H, Maruyama K. Machine learning-based risk model using ^{123}I-metaiodobenzylguanidine to differentially predict modes of cardiac death in heart failure. J Nucl Cardiol 2022; 29: 190–201.
9. Nakajima K, Nakata T, Yamada T, et al. A prediction model for 5-year cardiac mortality in patients with chronic heart failure using ^{123}I-metaiodobenzylguanidine imaging. Eur J Nucl Med Mol Imaging 2014; 41: 1673–82.
10. Orimo S, Suzuki M, Inaba A, Mizusawa H. ^{123}I-MIBG myocardial scintigraphy for differentiating Parkinson's disease from other neurodegenerative parkinsonism: A systematic review and meta-analysis. Parkinsonism Relat Disord 2012; 18: 494-500.
11. McKeith IG, Boeve BF, Dickson DW, et al. Diagnosis and management of dementia with Lewy bodies: Fourth consensus report of the DLB Consortium. Neurology 2017; 89: 88–100.
12. Yamada M, Komatsu J, Nakamura K, et al. Diagnostic criteria for dementia with lewy bodies: Updates and future directions. J Mov Disord 2020; 13: 1–10.
13. Nakajima K, Yamada M. ^{123}I-meta-iodobenzylguanidine sympathetic imaging: Standardization and application to neurological diseases. Chonnam Med J 2016; 52: 145–50.
14. Klene C, Jungen C, Okuda K, et al. Influence of ROI definition on the heart-to-mediastinum ratio in planar ^{123}I-MIBG imaging. J Nucl Cardiol 2018; 25: 208–16.
15. Okuda K, Nakajima K, Hosoya T, et al. Semi-automated algorithm for calculating heart-to-mediastinum ratio in cardiac Iodine-123 MIBG imaging. J Nucl Cardiol 2011; 18: 82–9.
16. Tilkemeier PL, Bourque J, Doukky R, Sanghani R, Weinberg RL. ASNC imaging guidelines for nuclear cardiology procedures: Standardized reporting of nuclear cardiology procedures. J Nucl Cardiol 2017; 24: 2064–128.
17. Soman P, Travin MI, Gerson M, Cullom SJ, Thompson R. I-123 MIBG cardiac imaging. J Nucl Cardiol 2015; 22: 677–85.
18. Flotats A, Carrió I, Agostini D, et al. Proposal for standardization of ^{123}I-metaiodobenzylguanidine (MIBG) cardiac sympathetic imaging by the EANM Cardiovascular Committee and the European Council of Nuclear Cardiology. Eur J Nucl Med Mol Imaging 2010; 37: 1802–12.
19. Chen J, Garcia EV, Galt JR, Folks RD, Carrio I. Optimized acquisition and processing protocols for I-123 cardiac SPECT imaging. J Nucl Cardiol 2006; 13: 251–60.
20. Dickson JC, Armstrong IS, Gabiña PM, et al. EANM practice guideline for quantitative SPECT-CT. Eur J Nucl Med Mol Imaging 2023; 50: 980–95.
21. Nakajima K, Okuda K, Matsuo S, Wakabayashi H, Kinuya S. Is ^{123}I-metaiodobenzylguanidine heart-to-mediastinum ratio dependent on age? From Japanese Society of Nuclear Medicine normal database. Ann Nucl Med 2018; 32: 175–81.
22. Nakajima K, Scholte AJHA, Nakata T, et al. Cardiac sympathetic nervous system imaging with ^{123}I-meta-iodobenzylguanidine: Perspectives from Japan and Europe. J Nucl Cardiol 2017; 24: 952–60.
23. Saito S, Nakajima K, Edenbrandt L, Enqvist O, Ulén J, Kinuya S. Convolutional neural network-based automatic heart segmentation and quantitation in ^{123}I-metaiodobenzylguanidine SPECT imaging. EJNMMI Res 2021; 11: 105.